Angewandte Chemie
Eine Zeitschrift der Gesellschaft Deutscher Chemiker

Supporting Information

Freeze–Thaw-Promoted Fabrication of Clean and Hierarchically Structured Noble-Metal Aerogels for Electrocatalysis and Photoelectrocatalysis

Ran Du, Jan-Ole Joswig, René Hübner, Lin Zhou, Wei Wei, Yue Hu, and Alexander Eychmüller**

anie_201916484_sm_miscellaneous_information.pdf

Author Contributions

W.W. Investigation: Equal.

Experimental Procedures

Reagents and Materials

Reagents including hydrogen tetrachloroaurate (III) ($HAuCl_4 \cdot 3H_2O$), silver nitrate ($AgNO_3$), potassium tetrachloropalladate (II) (K_2PdCl_4), potassium tetrachloroplatinate (II) (K_2PtCl_4), ammonium hexachlororhodate (III) ($(NH_4)_3RhCl_6$), trisodium citrate dihydrate (NaCA), sodium borohydride ($NaBH_4$), 20% palladium on carbon, and others were purchased from Sigma-Aldrich or Alfa-Aesar. All reagents are used without further purification.

Fabrication of Noble Metal Hydrogels (NMHs)

Hydrogels were synthesized by a freeze-thaw process, starting from the metal nanoparticle (NP) solutions. If not specified, the freezing process was performed by using liquid nitrogen. Bimetallic hydrogels were synthesized similar to the route for single-metal hydrogels, except that two metal precursor salts (at an equal molar ratio) were reduced together to form a multimetallic NP solution to serve as the precursor solution.

As an example, the fabrication of gold gels is illustrated. The gold NP solution was prepared by adding $HAuCl_4 \cdot 3H_2O$ solution (32.5 mM, 77.0 μL) to water (4.87 mL), followed by the addition of freshly prepared $NaBH_4$ aqueous solution (1.0 M, 50.0 μL). After 5 min, the resulting gold NP solution (metal salt concentration c_M = 0.5 mM) was flash-frozen by liquid nitrogen (−196 ºC, *ca.* 5 min). Then the sample was pre-thawed at room temperature (10–20 ºC) for 10 min and then fully thawed in a water bath (25–30 ºC) for 5 min. Afterwards, the sample was grounded for 12–24 h to allow the formation of a monolithic gel. For gels prepared in the presence of salts, the specific salt was introduced in the NP solution (salt concentration is 5 mM) before the freeze-thaw process, while other procedures were kept the same.

For scale-up production, the metal NP solution (800 mL) was prepared in a 1 L vessel, then the solution was distributed into several 100 mL vessels for further freeze-thaw treatment. The freezing time was *ca.* 15 min, while the pre-thawing and thawing time were *ca.* 15 min and 1 h, respectively.

Fabrication of Noble Metal Aerogels (NMAs)

The as-prepared hydrogels were washed by a large amount of water for 4–5 times with a total duration of 2–3 days to remove possible residues. Later on, hydrogels were solvent-exchanged at 303 K with tert-butanol for 2 times. Afterwards, the resulting wet gels were flash-frozen by liquid nitrogen and remained at −196 ºC for ~10 min to enable complete freezing. The frozen samples were put into the chamber of a freeze dryer (TOPTI-12S-80), performing the drying process at ~1 Pa for 12–24 h, where the temperature of the cold trap

was set to −80 ºC. The yield of NMAs was calculated based on the mass of the final aerogels with reference to the mass of the corresponding precursor metal salts.

Computational Procedures

Monte Carlo (MC) simulations

A self-developed random-walk Monte-Carlo algorithm was used for simulating the influence of disturbances on the gelation process. The initial positions of the particles (the particle radius was arbitrarily set to 3 nm) were generated randomly in a spherical space. All particles were non-interacting. For a spherical space with a volume of 1.07×10^7 nm^3 (sphere radius = 136.8 nm) and 50 particles, the corresponding particle concentration is denoted as c_0. Four particle concentrations, i.e. c_0, 5 c_0, 20 c_0, and 50 c_0, were adopted by changing the space volume (radius: 136.8, 80.0, 50.4, 37.1 nm, respectively). In each Monte-Carlo step, all particles (or aggregates) were either moved translationally or rotated (both with a probability of 50%). If – during translation or rotation – two particles (or aggregates) met, they were considered as one rigid aggregate afterwards. The algorithm was terminated if all particles were aggregated to one single aggregate. Translational movements were performed with a randomly chosen step length (between 0 nm and the maximum step length x). Rotations were performed with a randomly chosen rotation angle (between 0° and 10°).

For the calculation of the radius of gyration (R_g), all single particles were neglected (for point-like particles, $R_g = 0$) and only aggregates (with 2 or more particles) were considered. For the calculation of R_g from a not fully aggregated system (consisting of 2 or more aggregates), the radius of gyration is averaged over all aggregates. The radius of gyration of a single aggregate is calculated as:

$$R_g = \sqrt{\lambda_x^2 + \lambda_y^2 + \lambda_z^2}$$

where λ_x^2, λ_y^2, λ_z^2 are the eigenvalues of the diagonalized radius-of-gyration tensor of the n-particle aggregate:

$$G = \frac{1}{n}\sum_{i=1}^{n}\begin{pmatrix} x_i x_i & x_i y_i & x_i z_i \\ y_i x_i & y_i y_i & y_i z_i \\ z_i x_i & z_i y_i & z_i z_i \end{pmatrix}$$

For each parameter set, 1000 MC runs were performed for statistical analysis.

Characterizations

Microscopy Characterization

Scanning electron microscopy (SEM) analysis was performed on a Zeiss Gemini 500 or a Nova 200 NanoSEM scanning electron microscope. Samples were prepared by directly sticking them on conductive tape.

Transmission electron microscopy (TEM) analysis was carried out by using a FEI Tecnai G2 20 or a JEM-2100F microscope operated at 200 kV. HRTEM analysis was performed on a FEI Talos F200X microscope operated at 200 kV. Samples were prepared by dispersing in acetone under ultrasonication (15 s to 120 s, depending on their dispersing ability), followed by dropping onto carbon-coated copper grids and drying at ambient temperature.

High-angle annular dark-field scanning transmission electron microscopy (HAADF-STEM) imaging and spectrum imaging based on energy-dispersive X-ray spectroscopy (EDX) were performed at 200 kV with a Talos F200X microscope equipped with an X-FEG electron source and a Super-X EDX detector system (FEI). Prior to STEM analysis, the specimen mounted in a high-visibility low-background holder was placed for 2 s into a Model 1020 Plasma Cleaner (Fischione) to remove possible contamination.

Diffraction Characterization

X-ray powder diffraction (XRD) was carried out in reflection mode on a Siemens D5000 X-ray diffractometer operated at a voltage of 30 kV and a current of 10 mA with Cu Kα radiation (λ = 1.5406 Å). The data was collected in the range of 20°–90° (2θ) with a step size of $\Delta 2\theta$ = 0.02°. The sample was fixed on the holder by Scotch tape. For the single-metal system, the crystallite size was estimated by the Scherrer equation applying a crystallite-shape factor K = 0.9.

Spectroscopy Characterization

Ultraviolet–visible spectroscopy (UV-vis) absorption spectra were recorded on a Cary 60 UV-Vis Spectrophotometer.

Element Analysis

Inductively coupled plasma optical emission spectroscopy (ICP-OES) was performed on a Perkin-Elmer Optima 7000DV optical emission spectrometer.

Gas Adsorption Measurement

Nitrogen adsorption experiments were performed with a Quantachrome NOVA 3000e system at 77 K. The sample was outgassed at 323 K for ~24 h under vacuum before measurement. The filling rod was used to reduce the dead volume, thus improving the measurement accuracy. The specific surface area was calculated by using the multi-point Brunauer–Emmett–Teller (BET) equation ($0.1 < p/p_0 < 0.3$). The pore size distribution was derived by using the non-local density functional theory (NLDFT) method (N_2 at 77 K on carbon) based on a slit pore geometry. The total pore volume was calculated at $p/p_0 = 0.99$, similar to the value derived by the BJH (Barret–Joyner–Halender) method.

Electrochemical Measurements

All electrochemical measurements were performed with a three-electrode system on an Autolab/PGSTAT 30 (Eco Chemie B. V. Utrecht, the Netherlands) or a CHI potentiostat (CHI 760D). A glassy carbon electrode (GCE, 3 mm in diameter), an Ag/AgCl (saturated KCl aqueous solution) electrode, and a platinum foil were used as working electrode, reference electrode, and counter electrode, respectively.

For modification of the working electrode, ~1.0 mg catalyst was dispersed in 425 μL 2-propanol (IPA) and 75 μL Nafion (1 wt.% in IPA) by sonicating for ca. 30 min to acquire the catalyst ink. Then a specific amount of ink was transferred on the GCE and evaporated at ambient temperature. The concentration of Pd and Pt in the ink were determined by ICP-OES, and the total loading of Pd or Pt was calculated accordingly to ~20 μg cm^{-2}.

For the electro-oxidation of ethanol, the measurement was performed under N_2 atmosphere in 1.0 M KOH aqueous solution containing 1.0 M ethanol. CV curves were recorded between −0.9 and 0.3 V (*vs.* AgCl/Ag) with a scanning rate of 50 mV s^{-1}. The stability test was conducted at a potential of −0.23 V (*vs.* AgCl/Ag). For the photoelectrocatalysis, a round panel with seven LED lamps (7×OSRAM SSL 80 Streetwhite on round PCB (provided by LED. Tech. Color: 5700–7500 K, wavelength 350–800 nm, the diameter of the panel is 35 mm, LEDs are evenly distributed on the panel) was closely placed under the electrolytic cell. The LEDs were lightened by a tunable power source. The light power density (0–133.6 mW cm^{-2}) was calibrated by an optical power meter assuming an even light field distribution and neglecting the interactions between light and the electrolyte solution. For each sample, at least three measurements were conducted, and one set of typical data was used.

Figures

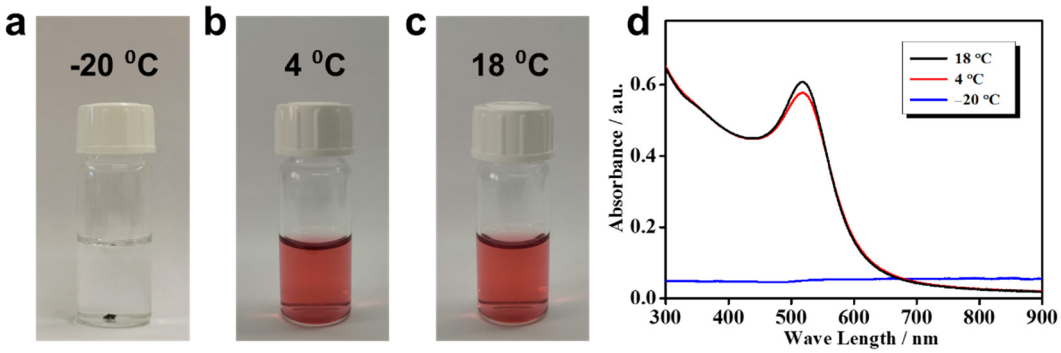

Figure S1. Photographs of Au NP solutions (c_M = 0.2 mM) after the freeze-thaw with the freezing temperature at (a) -20 ºC (in a fridge), (b) 4 ºC (in a fridge), and (c) room temperature (~18 ºC). (d) The corresponding UV-vis spectra of those solutions after processing under different temperatures.

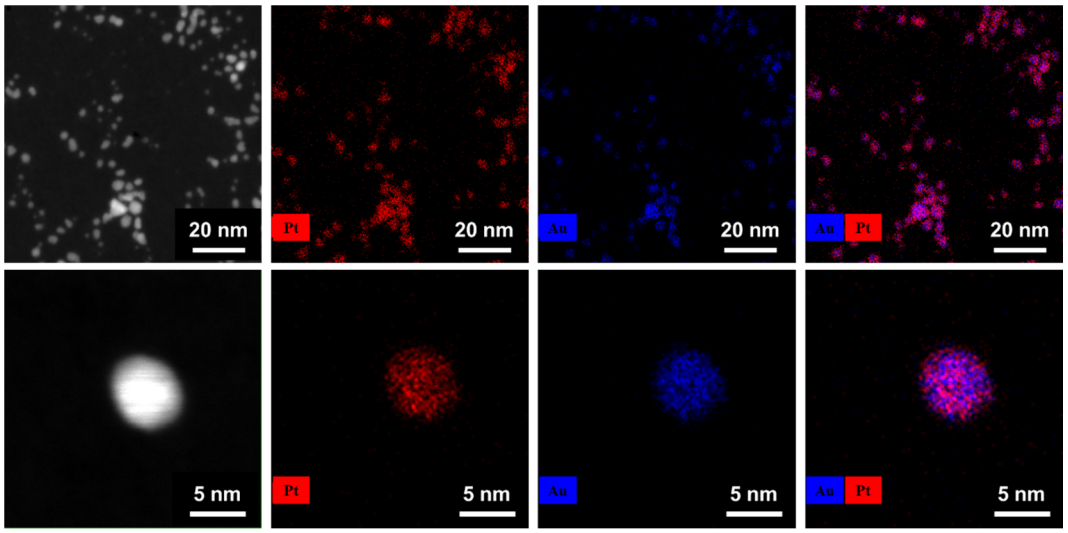

Figure S2. HAADF-STEM images and the corresponding EDX mappings of the Au-Pt precursor NPs at different magnification, indicating a homogeneous elemental distribution.

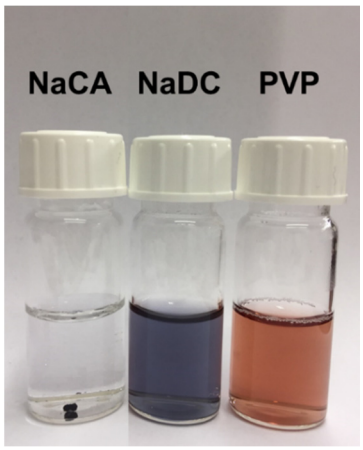

Figure S3. Photographs of Au NP solutions after the freeze-thaw process. The initial Au NP solutions were stabilized by trisodium citrate (NaCA), sodium deoxycholate (NaDC), and polyvinyl pyrrolidone (PVP), respectively.

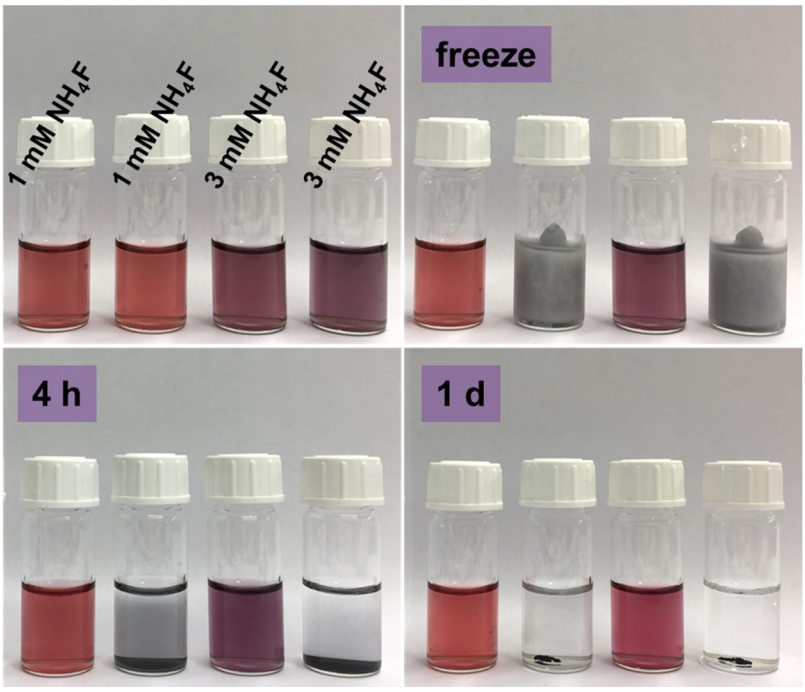

Figure S4. Photographs of Au NP solutions with the presence of the indicated salts, at room temperature (1st and 3rd vial) and during the freeze-thaw process by liquid nitrogen (2nd and 4th vial).

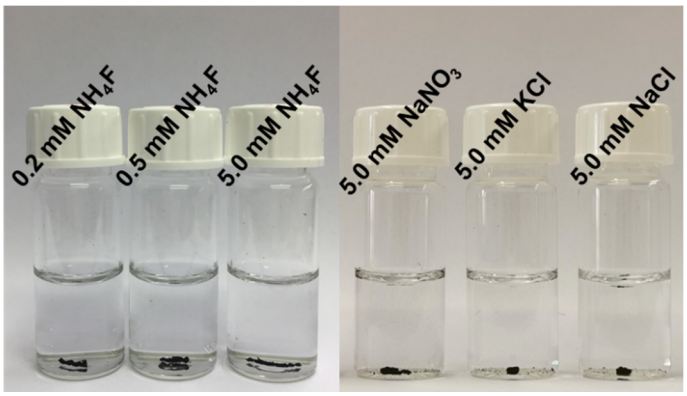

Figure S5. Photographs of Au NP solutions after the freeze-thaw treatment with the presence of the indicated salts.

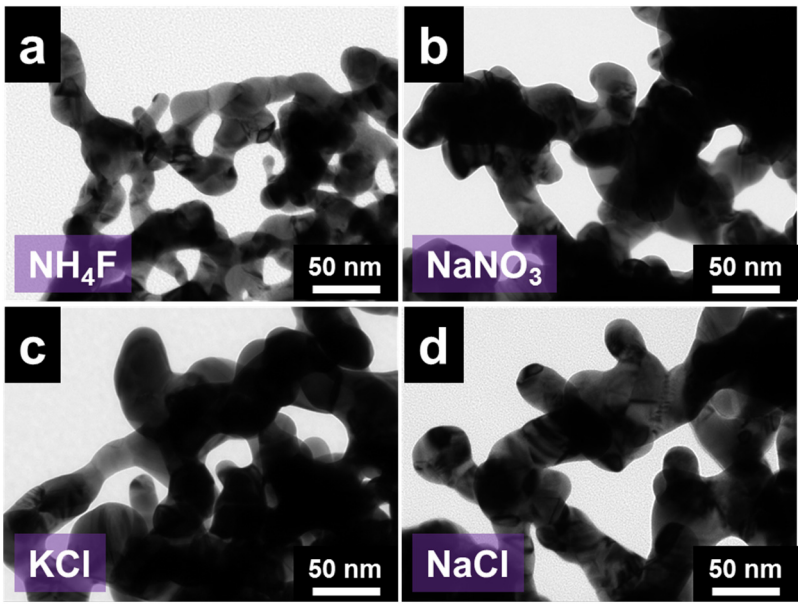

Figure S6. TEM images of freeze-thaw-directed aerogels with the presence of 5 mM of the indicated salt.

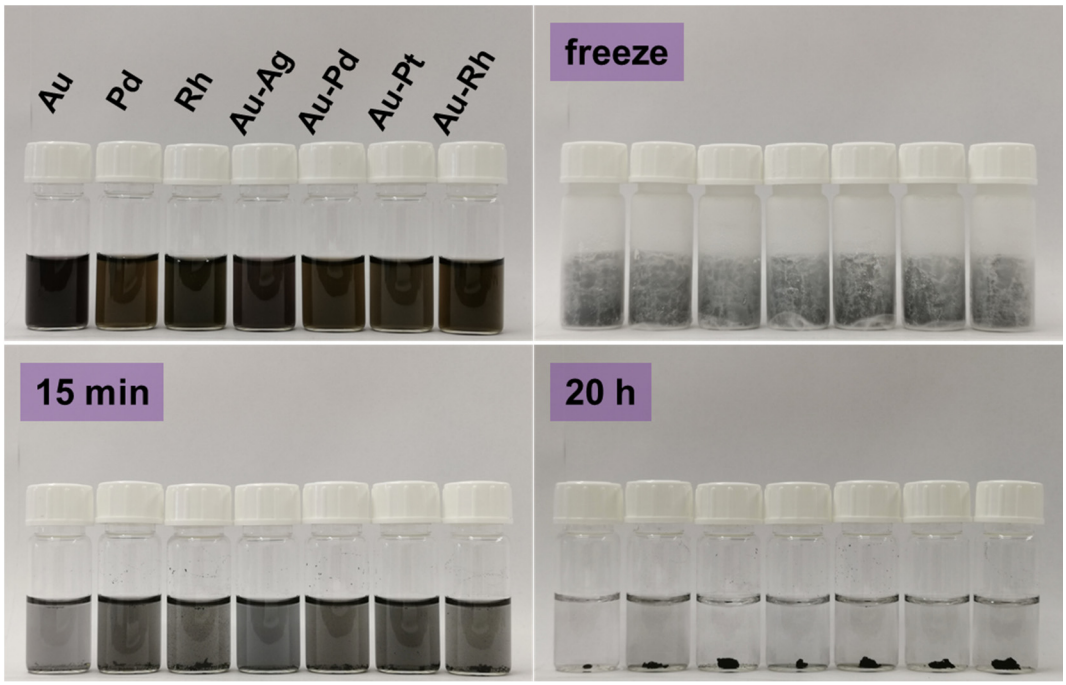

Figure S7. Photographs of the freeze-thaw-directed gelation process of NMAs with different compositions.

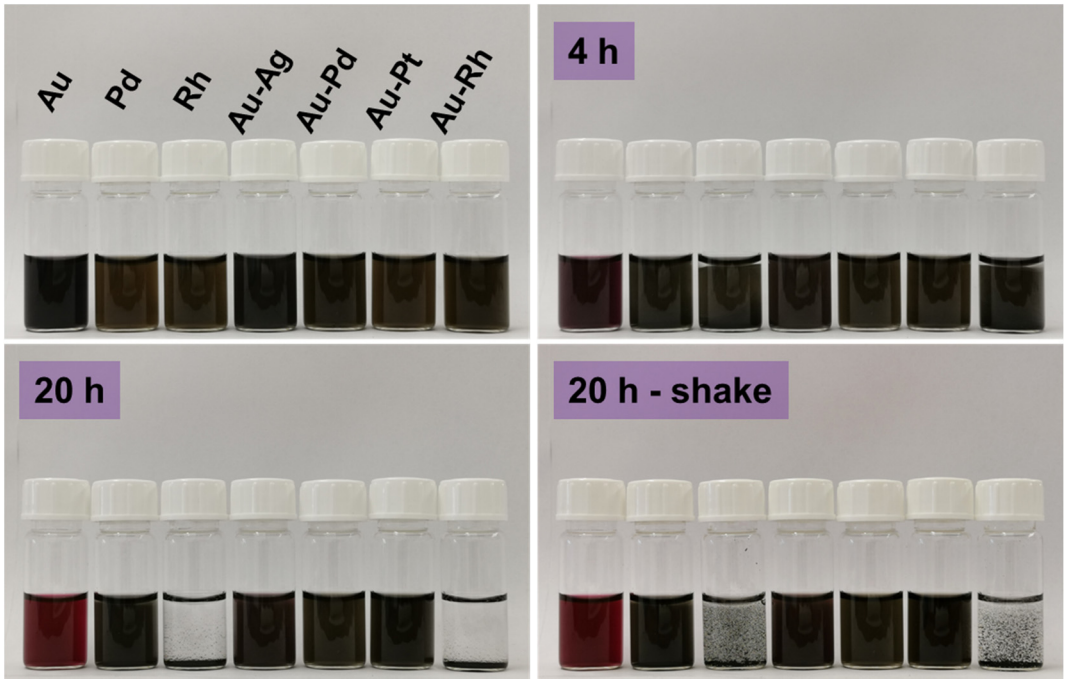

Figure S8. Photographs of the stability of diverse noble metal NP solutions at room temperature.

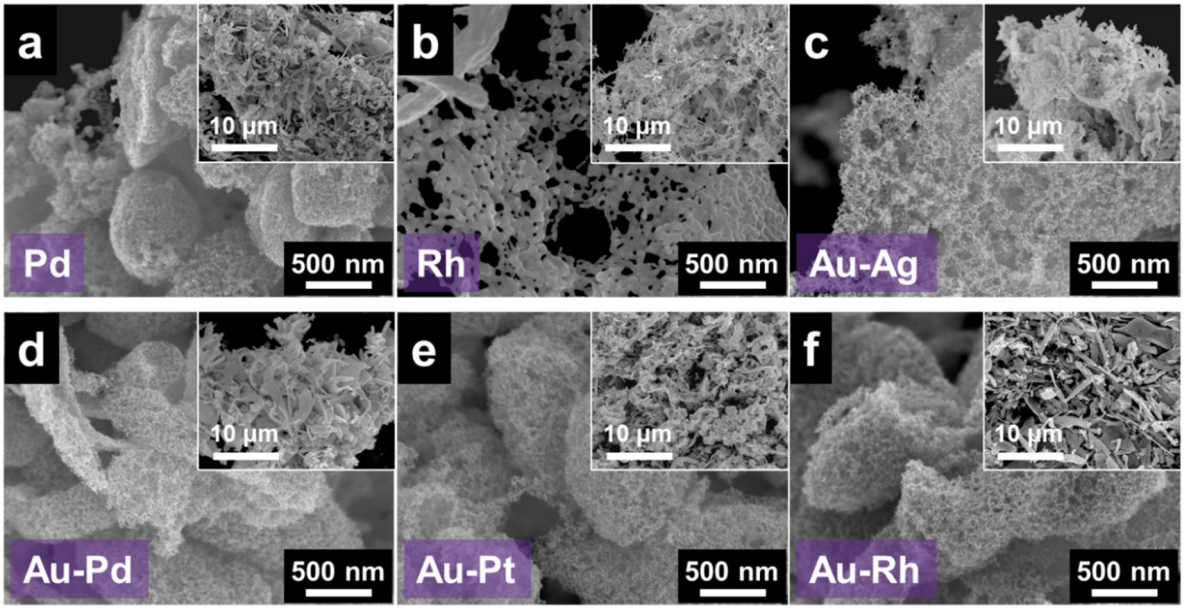

Figure S9. SEM images of diverse mono- and bimetallic aerogels.

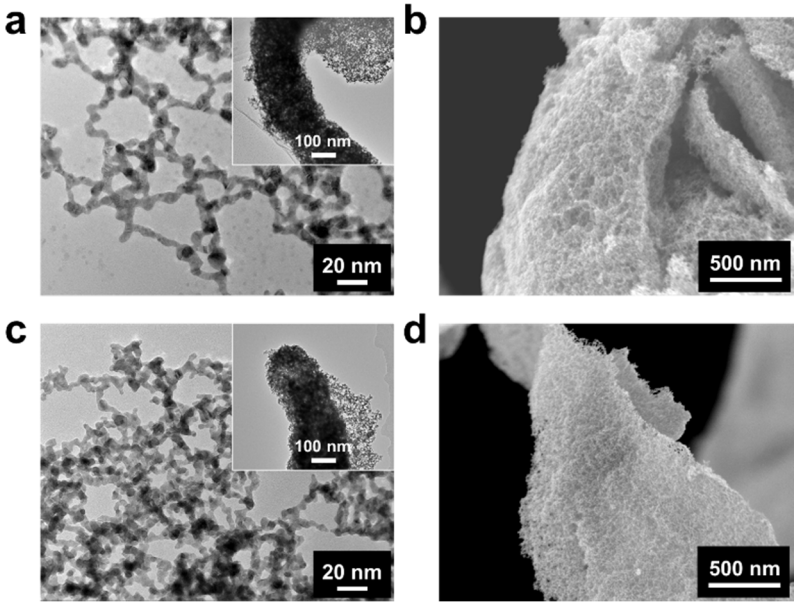

Figure S10. TEM images and SEM images of (a-b) Au-Pd and (c-d) Au-Pt aerogels prepared from supercritical drying of as-obtained hydrogels.

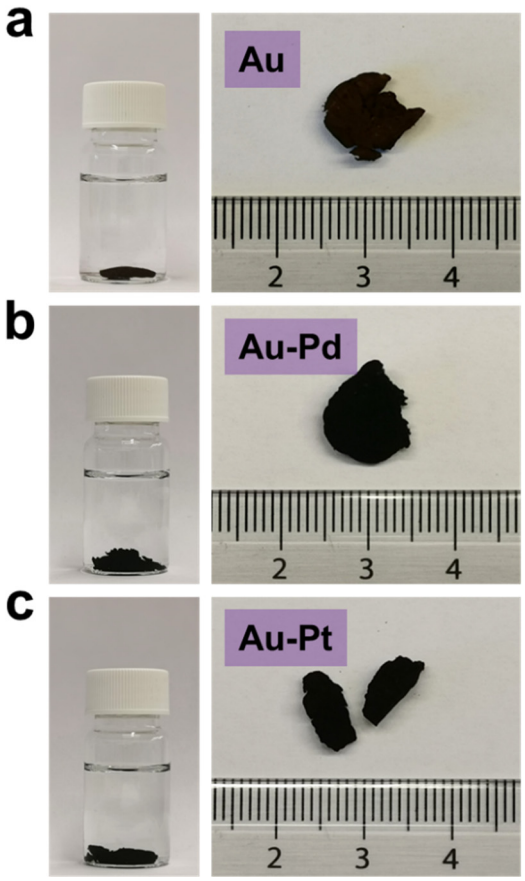

Figure S11. Photographs of noble metal hydrogels and aerogels made of (a) Au, (b) Au-Pd, and (c) Au-Pt.

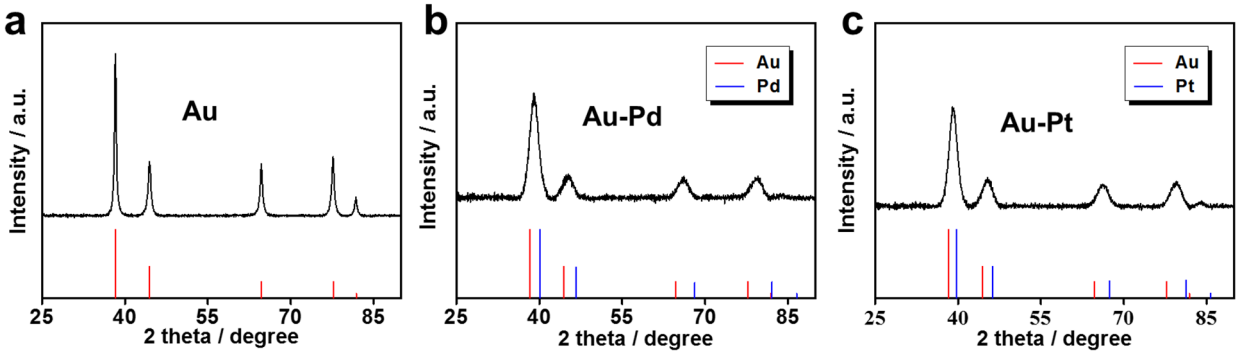

Figure S12. XRD patterns of diverse aerogels made of (a) Au, (b) Au-Pd, and (c) Au-Pt.

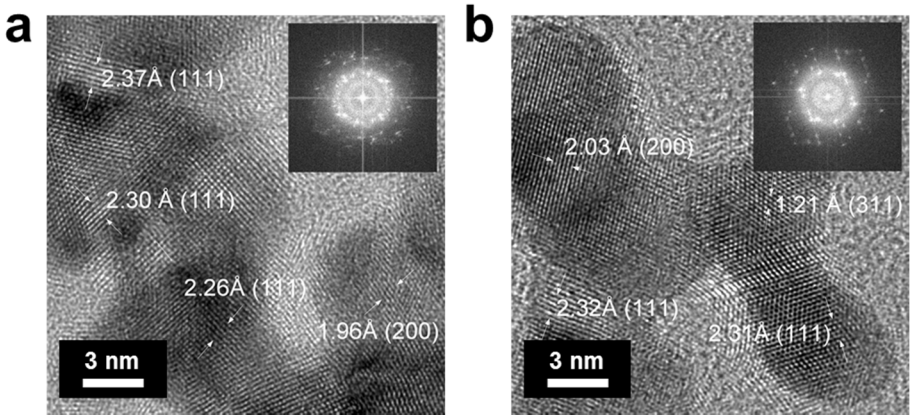

Figure S13. HR-TEM of the (a) Au-Pt and (b) Au-Pd aerogels. The insets are the corresponding diffractograms derived by Fast Fourier Transform (FFT) analysis of the HR-TEM images. It is worth pointing out that the inter-diffusion of the two metals can lead to a certain-degree deviation of the lattice parameters and hence the corresponding lattice spacings between the values of the original metals.

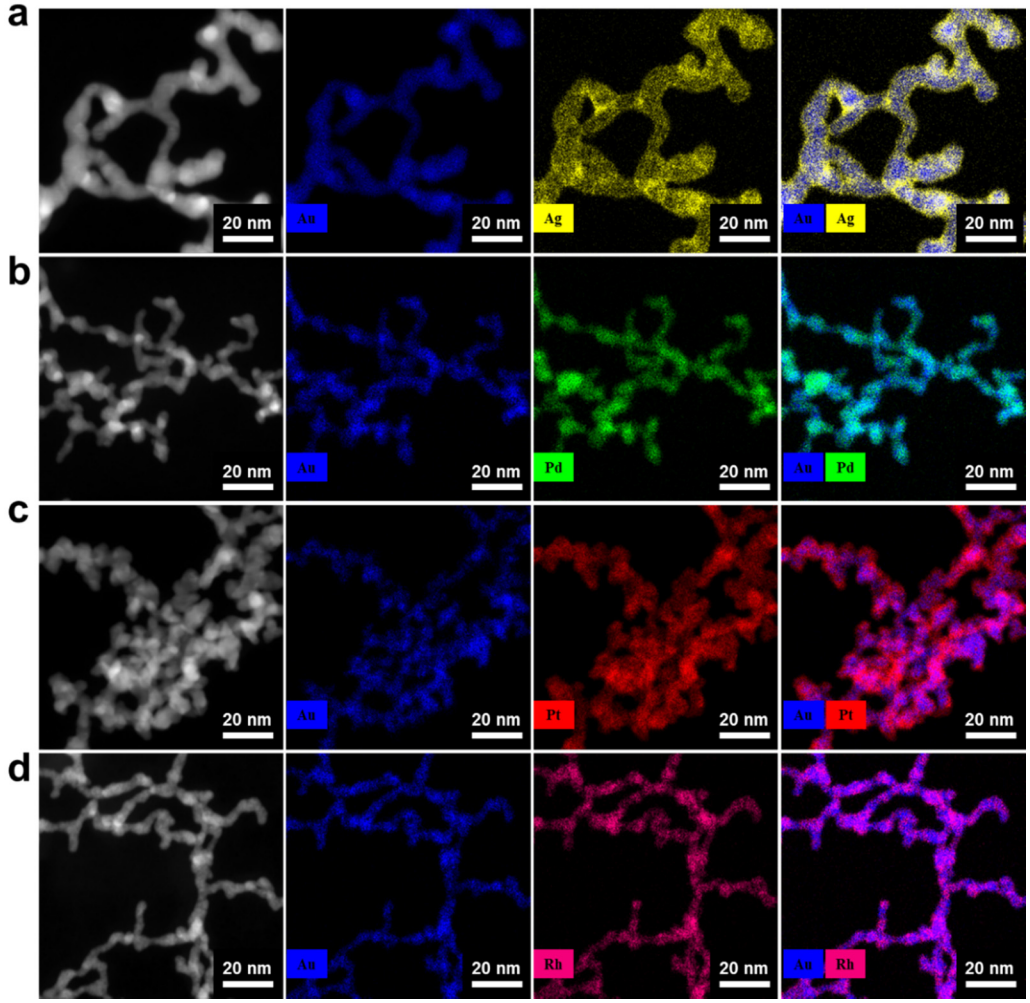

Figure S14. HAADF-STEM imaging and corresponding EDX mapping of multimetallic aerogels, (a) Au-Ag, (b) Au-Pd, (c) Au-Pt, and (d) Au-Rh.

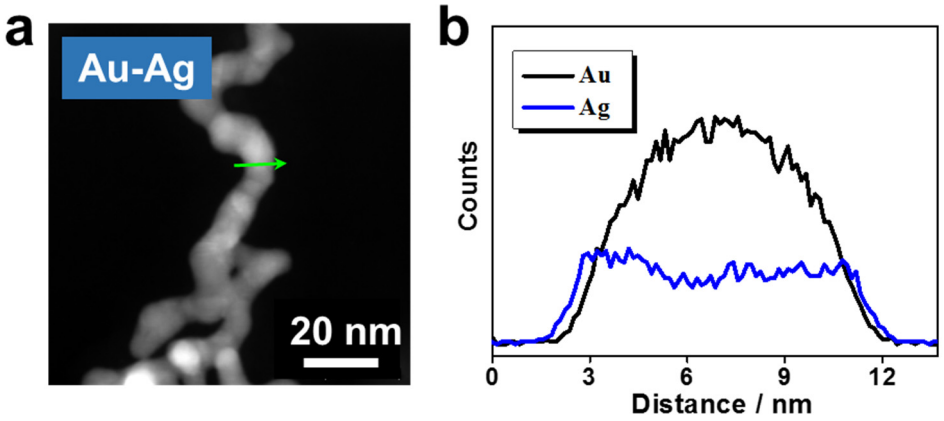

Figure S15. HAADF-STEM imaging and EDX analysis (line scan) of the core-shell-structured Au-Ag aerogel.

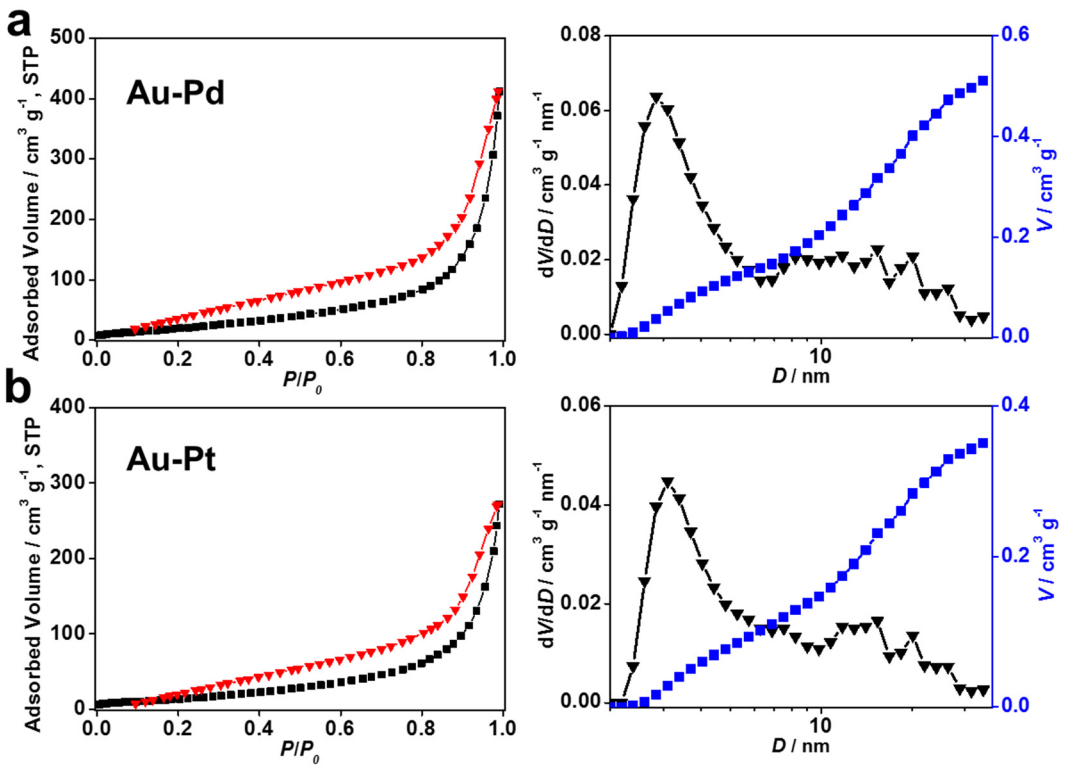

Figure S16. Adsorption/desorption isotherms and pore size distributions of several bimetallic aerogels, (a) Au-Pd, (b) Au-Pt.

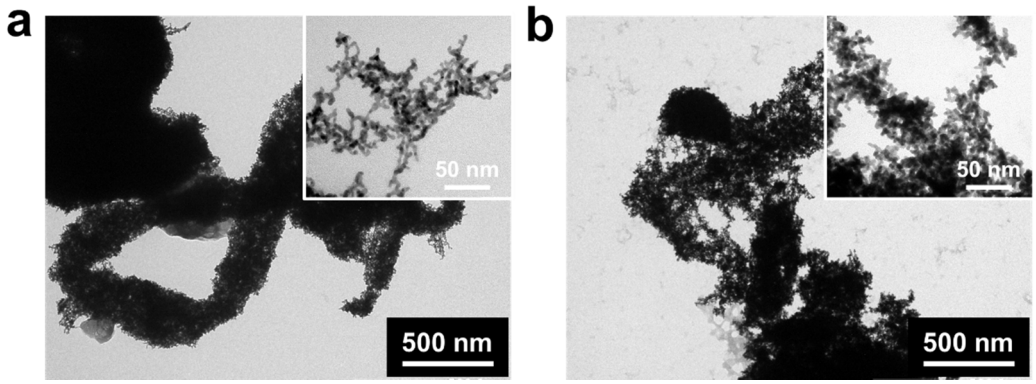

Figure S17. TEM images of (a) Au-Pd and (b) Au-Pt based catalyst ink prepared by sonicating the corresponding aerogels with Nafion.

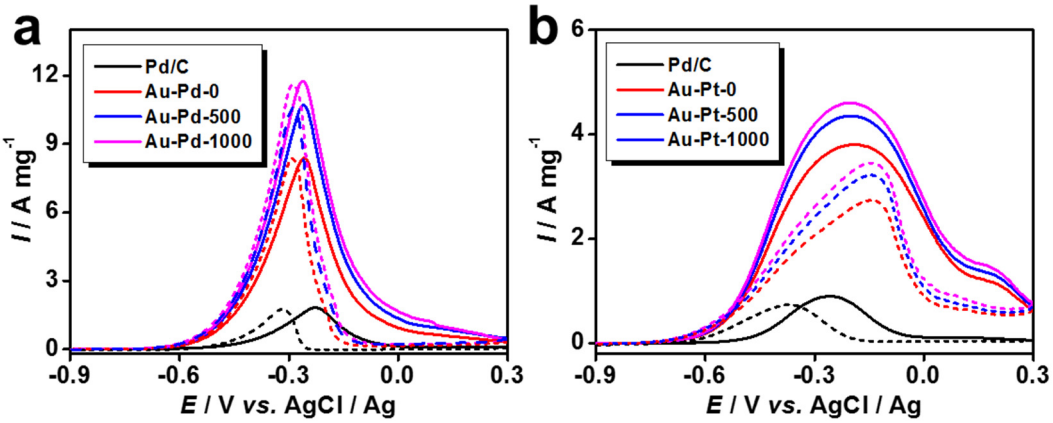

Figure S18. Characterization of the photoelectrocatalytic EOR properties of (a) the Au-Pd and (b) the Au-Pt aerogel. The suffix 0, 1, and 2 denotes that the measurement was conducted under light illumination with a power density of 0, 64.1, and 133.6 mW cm^{-2}, respectively. Commercial Pd/C and Pt/C catalysts were tested in dark condition. All tests were performed in N_2-saturated 1.0 M KOH + 1.0 M ethanol solution at a scan rate of 50 mV s^{-1}.

Tables

Table S1. Summary of parameters of as-prepared aerogels in this work. The specific surface area S_{BET} (m^2 g^{-1}) was calculated in the partial pressure (p/p_0) range of 0.1–0.3. The total pore volume V_{tot} was derived at p/p_0=0.99. The average ligament size d was obtained from a statistic analysis of TEM images. The density was estimated by averaging the values from at least 3 aerogels with relatively regular shapes, d was obtained by averaging at least 30 measurements from two batches of samples, and S_{BET} and V_{tot} were confirmed by at least two separate measurements.

Entry	Metals	Additives[b]	S_{BET} (m^2 g^{-1})	V_{tot} (cm^3 g^{-1})	d (nm)	Density (mg cm^{-3})
1	Au	/	/	/	35.0 ± 7.2	164.4 ± 24.6
2	Au[b]	NH_4F	/	/	16.8 ± 3.2	/
3	Au[b]	$NaNO_3$	/	/	28.0 ± 4.7	/
4	Au[b]	KCl	/	/	29.2 ± 5.9	/
5	Au[b]	NaCl	/	/	32.3 ± 6.3	/
6	Pd	/	/	/	4.5 ± 0.6	/
7	Rh	/	/	/	4.8 ± 0.7	/
8	Au-Ag	/	/	/	7.2 ± 1.1	/
9	Au-Pd	/	83.6	0.526	4.3 ± 0.8	35.9 ± 4.0
10	Au-Pt	/	74.5	0.475	4.7 ± 0.8	60.6 ± 5.5
11	Au-Rh	/	/	/	3.3 ± 0.4	/

[a] If not specified, the metal nanoparticle solutions were directly used for the freeze-thaw process.

[b] The concentration of the metal salt precursor is 0.2 mM. For other formulas which are not specified, the concentration is 0.5 mM.

Table 2. Summary of fabrication strategies and physical properties of various NMAs.

Metals	Methods	Gelation Time	Density (mg cm^{-3})	Size (nm)	Surface area (m^2 g^{-1})	Ref
Au, Pd, Rh, Au-Ag, Au-Pd, Au-Pt, Au-Rh	Freeze-thaw	12-24 h	35.9-164.4	3.3-35.0	74.5-83.6 for Au-Pd and Au-Pt aerogels	This work
Au	Chemical dealloying	/.	/	20-40	3.7	1
Au	Combustion synthesis	/	57	10-100	10.9	2
Pd			/	10-20	36.5	
			/			
Au	Conc,[a] direct freeze drying	/	20-60	200-500	/	3
Ag				10-50	15	
Pd				3-7	15	
Pt				3-10	33	
Au	Dopamine	6-72 h	40-43	5-6	up to 50.1	4
Ag	Conc,[a] $C(NO_2)_4$	4-12 h	37-41	5-11[b]	43-160	5
Pd	Conc,[a] Ca^{2+}	5 min to 2 month	25-59	3-10	40-108	6
Au	Precursor 5-100 mM, $NaBH_4$, NaH_2PO_2, or dimethylamine borane	A few minutes	540	18-280	3.1	7
Pd			65	12-65	15.4	
Pt			55	13-60	20.6	
Au-Ag, Ag-Pt	Conc[a], H_2O_2	8-15 d	16	3-10	46-48	8
Au, Pd, Au-Ag, Au-Pd, Au-Pt, Pd-Pt, Au-Pd-Pt	Precursor 0.02-2 mM, Salts	2-48 h	61.4-212.8	3.1-113.7	2.5-122.7	9
Au-Ag	Conc,[a] $C(NO_2)_4$	4-6 h	51-55	6-60	67-73	10
Au-Ag, Pd-Ag, Pt-Ag	Conc,[a] rotary evaporation or NaCl	1-28 d	10-180	13.0-15.4	32–42	11
AuCu, PdCu, PtCu	$NaBH_4$, 333 K	6 h	/	5-6	21.3-37.5	12
Pd-Ni	Conc,[a] $NaBH_4$,	< 6h	35	2-5[b]	95.4	13

	348 K					
Ir_xCu	$NaBH_4$, 343 K	2-3 h	/	3-7	41.7	14
Au	Excessive $NaBH_4$	2-12 h	60.5-576.5	4.8-38.3	3.5-59.8	15
Ag, Pt, Os			157.2-250.6	48.2-226.7	2.1-13.2	
Ru, Rh, Au-Ru			/	3.9-5.5	/	
Pd, Au-Ag, Au-Pd, Au-Pt, Au-Ru, Au-Rh, Au-Ir			46.7-169.8	4.3-7.6	42.6-72.9	

[a] Estimated sizes from SEM or TEM images.

[b] The size of primary nanoparticles of aerogels.

References

1. V. Zielasek, B. Jürgens, C. Schulz, J. Biener, M. M. Biener, A. V. Hamza, M. Bäumer, *Angew. Chem. Int. Ed.* **2006**, *45*, 8241-8244.
2. B. C. Tappan, S. A. Steiner, E. P. Luther, *Angew. Chem. Int. Ed.* **2010**, *49*, 4544-4565.
3. A. Freytag, S. Sánchez-Paradinas, S. Naskar, N. Wendt, M. Colombo, G. Pugliese, J. Poppe, C. Demirci, I. Kretschmer, D. W. Bahnemann, P. Behrens, N. C. Bigall, *Angew. Chem. Int. Ed.* **2016**, *55*, 1200-1203.
4. D. Wen, W. Liu, D. Haubold, C. Zhu, M. Oschatz, M. Holzschuh, A. Wolf, F. Simon, S. Kaskel, A. Eychmüller, *ACS Nano* **2016**, *10*, 2559-2567.
5. X. Gao, R. J. Esteves, T. T. H. Luong, R. Jaini, I. U. Arachchige, *J. Am. Chem. Soc.* **2014**, *136*, 7993-8002.
6. D. Wen, A.-K. Herrmann, L. Borchardt, F. Simon, W. Liu, S. Kaskel, A. Eychmüller, *J. Am. Chem. Soc.* **2014**, *136*, 2727-2730.
7. F. J. Burpo, E. A. Nagelli, L. A. Morris, J. P. McClure, M. Y. Ryu, J. L. Palmer, *J. Mater. Res.* **2017**, *32*, 4153-4165.
8. N. C. Bigall, A. K. Herrmann, M. Vogel, M. Rose, P. Simon, W. Carrillo-Cabrera, D. Dorfs, S. Kaskel, N. Gaponik, A. Eychmüller, *Angew. Chem. Int. Ed.* **2009**, *48*, 9731-9734.
9. R. Du, Y. Hu, R. Hübner, J.-O. Joswig, X. Fan, A. Eychmüller, *Sci. Adv.* **2019**, *5*, eaaw4590.
10. X. Gao, R. J. A. Esteves, L. Nahar, J. Nowaczyk, I. U. Arachchige, *ACS Appl. Mater. Interfaces* **2016**, *8*, 13076-13085.
11. K. G. Ranmohotti, X. Gao, I. U. Arachchige, *Chem. Mater.* **2013**, *25*, 3528-3534.
12. C. Zhu, Q. Shi, S. Fu, J. Song, H. Xia, D. Du, Y. Lin, *Adv. Mater.* **2016**, *28*, 8779-8783.
13. B. Cai, D. Wen, W. Liu, A. K. Herrmann, A. Benad, A. Eychmüller, *Angew. Chem. Int. Ed.* **2015**, *54*, 13101-13105.

14. Q. Shi, C. Zhu, H. Zhong, D. Su, N. Li, M. H. Engelhard, H. Xia, Q. Zhang, S. Feng, S. P. Beckman, *ACS Energy Lett.* **2018**, *3*, 2038-2044.

15. R. Du, J. Wang, Y. Wang, R. Hübner, X. Fan, I. Senkovska, Y. Hu, S. Kaskel, A. Eychmüller, *Nat. Commun.* **2020**, 10.1038/s41467-41020-15391-w.